DOI 10.18524/1810-4215.2021.34.244335

APPLICATION OF PHOTOMETRY TO UNDERSTAND THE BEHAVIOUR OF GEOSTATIONARY OBJECTS ON ORBIT

P. P. Sukhov[1], V. P. Yepishev[2], I. I. Motrunich[2], K. P. Sukhov[3]

[1] Astronomical Observatory of I.I.Mechnikov Odesa National University, 65014, Ukraine, *psukhov@ukr.net*

[2] Space Research Laboratory of the Uzhgorod National University, 2a Dalekaya St, Uzhhorod, 88000, Ukraine, *lkd.uzhgorod@gmail.com*

[3] Ukrainian National Space Facilities Control and Test Centre, *sppete@ukr.net*

ABSTRACT. One of the challenges of satellite characterization is the ability to not only determine the spacecraft orbit, but also ssatellite operating status, orientation, size, bus type, and material properties. Positional observations allow us to determine and/or update orbital elements of satellites, but they do not afford an insight into the behaviour of a satellite in orbit.

The article discusses the results of solving the inverse problem of astrophysics. How you can use photometric, astrometric information about a satellite, its lighting conditions, supplemented by additional information, to understand the behavior of a satellite in orbit. The results are shown using examples of four satellites in geostationary orbit. An algorithm for calculating the photometric and dynamic characteristics of geostationary objects is provided.

Keywords: geostationary satellite; space surveillance awareness; light curve; multi-colour photometry.

АНОТАЦІЯ. Однією з проблем характеризації супутника є здатність не тільки визначати орбіту космічного корабля, але й робочий стан супутника, орієнтацію, розмір, тип шини та властивості матеріалу. Позиційні спостереження дозволяють нам визначати та/або оновлювати орбітальні елементи супутників, але вони не дозволяють зрозуміти поведінку супутника на орбіті. У статті розглядаються результати розв'язування оберненої задачі астрофізики. Як можна використовувати фотометричну, астрометричну інформацію про супутник, умови його освітлення, доповнену додатковою інформацією, щоб зрозуміти поведінку супутника на орбіті. Результати показані на прикладах чотирьох супутників на геостаціонарній орбіті. Надано алгоритм розрахунку фотометричних та динамічних характеристик геостаціонарних об'єктів.

Ключові слова: геостаціонарний супутник; поінформованість про космічний нагляд; крива блиску; багатоколірна фотометрія.

1. Introduction

An important task of space situational awareness is to continuously monitor satellite orbits and calculate orbital elements of space objects (SO). The term "behaviour of a geostationary satellite (GSS) at a given sub-point", adopted in this paper, refers to the following aspects:

- Satellite operational status: active, inactive, stable or unstable;
- The satellite breakdown or signs of its malfunction, such as failure to unfold aerials or solar arrays;
- Orientation (X,Y,Z) of the satellite external payload elements, including radio aerials, solar arrays;
- Failure to stabilise the satellite in a fixed orientation with respect to a given axis;
- Schedule of scanning the Earth**'s** regions by satellite payload elements;
- Changes over time in reflectance characteristics (reflectance degradation) of the SO surface.

Positional observations enable us to determine and/or update satellite orbital elements, but they do not allow to comprehensively describing of the satellite behaviour in orbit. These data can be inferred from combined photometric and astrometric observations.

Photometric, polarimetric and spectral observations provide information needed to identify an SO, such as details about the spacecraft payload with its specific functionalities and non-standard modes of operation, and to determine the SO orientation, period of rotation around the centre of mass, dimensions, surface material and schedule of the Earth's surface scanning. These characteristics, being used primarily to identify resident space objects, also allow us to determine some of their photometric and dynamic features.

Over the last decade, numerous papers regarding photometric observations of satellites have been published [1-15, etc.]. But multi-colour photometry proved to be the most useful in describing the behaviour of SO in geostationary orbit. However, this method has begun to progressively develop just in recent times and quite only a few articles have been published recently on this topic. However, this method only began to develop progressively recently, and few arti-

cles been published on this topic [16-23]. In a number of studies, researchers have attempted to automate the SO identification process, based on empirical astrometric and photometric data, using neural networks, as described, for instance, in reference [7]. However, due to a high complexity of this task, the reliability of identifications does not exceed 70-80%. In this paper, we focus on the potential capability of multi-colour photometry and show that it may be a powerful tool in studying the reflectance properties of the satellite surface and SO behaviour in orbit. It is worth noting that combining astrometric and multi-colour photometric data can yield a broader pattern of behaviour of the observed SO.

In this paper, we focus on the potential capability of multi-colour photometry and show that it may be a powerful tool in studying the reflectance properties of the satellite surface and characterising the SO behaviour in orbit. It is worth noting that combining astrometric and multi-colour photometric data can yield a broader pattern of behaviour of the observed SO.

Physical parameters acquired from the SO photometry can be divided into three groups, namely:

- *Photometric characteristics*: 1) the effective reflecting area, – ($S\gamma_\lambda$); 2) the spectral reflectance coefficient – γ_λ; 3) the phase coefficient, – β (Δm/deg); 4) colour-indices – *CI*, (B-V, V-R, B-R, etc.); 5) the reduced magnitude – m_λ, which is the magnitude at a given phase angle (usually $\psi = 0^0$ or $\psi = 25^0$) reduced to a distance of 36,000 km;
- *Opto-geometric characteristics*: 1) linear dimensions; 2) the prevailing shape; 3) the solar array size and power; 4) platform type, external payload composition;
- *Dynamic characteristics*: 1) the period of rotation about either the centre of mass or any of the axes; 2) instantaneous spatial orientation that is defined by the normal to the SO reflecting glint-producing surface specified with the X, Y and Z vector components.

All the characteristics listed above, except for the effective reflecting area ($S\gamma_\lambda$), can be derived from photometric observations using different sources. However, in fact, the problems of determining the behavior of SO in orbit from photometric observations are mathematically incorrect and ambiguous. To have a well-posed problem, the Tikhonov regularisation method should be applied [24]; to this end, we need to factor in some a priori information about studied SO. Such additional data may include the following details: dimensions of the satellite structural elements and their mutual orientation; the solar array power; the satellite launch date and type of platform (satellite bus); the Sun-SO-observer geometry; light curves; colour-indices; the rotation period and normal direction to the SO glinting surface; resulting solutions of dynamic numerical simulations; relevant findings reported by other researchers, etc. All these data may contribute to better understanding of the behaviour of orbiting SO. The concept of understanding the behaviour of SO in orbit is based on the comparison between physical parameters inferred from observations. These parameters are listed above.

2. Method, Experiment

We carried out observations using a high-speed photometer with a FEU-79 photomultiplier operating in a pulse-counting mode. Quoting Krantz [8], high-speed optical photometry of SO "is driving a renaissance in this field".

The observations were conducted with a 20-inch Cassegrain reflector. The electronic path of the photometer was calibrated with the current- and temperature-stabilised light-emitting diode AL-102 as a reference light source [25]. Standard BVR filters of the extended Johnson photometric system were employed. Calibration of the observations has been performed using the catalogue of WBVR magnitudes of bright northern sky stars [26], which contains high-precision data and provides more uniform coverage of the equatorial zone as compared with the Landolt catalogue.

For operational records, the instantaneous value of the extinction coefficient was determined by the method of two different zenith-distances of stars: the first star was observed near the zenith while the second one – near the celestial equator.

Photometric data processing and calculating physical parameters were carried out in the following stages:

- Determination of the GSS instrumental magnitude and its reduction to the standard Johnson-Morgan system;
- Calculation of the magnitude reduced to a distance of 36,000 km;
- Calculation of the phase angles ψ during each observing session and plotting the respective phase-folded light curves;
- Calculation of the effective reflecting area for the obtained phase angles; and
- Calculation of the magnitude, effective reflecting area and other physical characteristics GSS at $\psi = 0^0$ and $\psi = 25^0$.

From adopted positional and photometric observations, we determined the phase angle of the satellite – ψ, the apparent magnitude of the satellite within the relevant spectral range – m_λ, and the effective reflecting area – ($S\gamma_\lambda$). The normal vector to the satellite glinting surface was determined using a method described by Yepishev [3]. The effective reflecting area ($S\gamma_\lambda$) can be derived from the Equations 1 and 2 given in [5]:

$$m_\lambda = m_\lambda^\Theta - 2{,}5\lg\left[\frac{S\gamma_\lambda F(\psi)}{d^2}\right] \qquad (1)$$

$$S\gamma_\lambda = d^2 \cdot 10^{\frac{m_\lambda^\Theta - m_\lambda}{2.512}} \cdot \sec\psi \qquad (2)$$

Here m_λ^Θ - the Sun's magnitude in the spectral range. In the next section, we present the results obtained for four satellites that afford an insight into the behaviour of SO in orbit**.**

3. Results

Phobos-Grunt. Phobos-Grunt was an attempted Russian sample return mission to Phobos, which failed to set on a course for Mars and, having been stranded in a low Earth orbit, ultimately fell back to Earth in an uncontrolled re-entry [27]. The Phobos-Grunt positions during our observing sessions were calculated from the USSPACECOM (NORAD) catalogue data. Six light curves were plotted in total. Figure 1 presents a light curve of this SO in its transitional orbit plotted from observations conducted on 01 December 2011 at the Lviv Astronomical Observatory.

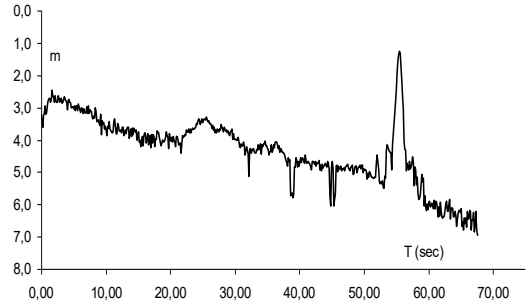

Figure 1: A light curve of Phobos-Grunt observed in the V band on 01 December 2011.

Processing and analysing the obtained observational data yielded the following details:

- The rotation period during our observing session was 67.86 sec;
- The SO rotation axis was directed almost vertically, that is, practically parallel to the zenith-nadir line, making an angle less than 10º with it;
- The angle between the SO rotation and longitudinal axes reached ~ 45º (as of 01 December 2011). As a result, the SO longitudinal axis with respect to the vertical (zenith-nadir) line and observer resembles a stretched spiral along the orbit that periodically deviates from its plane by 40º–52º;
- Only one solar array could be seen while the second one did not scatter the light towards the observer as it was shaded by the SO body throughout the observing session. The Sun illuminated the upper side of the solar arrays when the SO was passing over the Southern hemisphere;
- Due to a conical rotation of the SO body, the duration of charging on-board batteries by the solar arrays should be very short; and
- It appeared that during our observations of Phobos-Grunt, its spin-stabilisation system did not function properly. The data obtained from our computations may be useful in tracing the cause of the Phobos-Grunt entering the emergency mode.

DSP-18. Several Defence Support Programme (DSP) reconnaissance satellites can be observed from Ukrainian facilities. Four years of observations of these satellites yielded more than 40 light curves in the B,V,R bands It is known that a DSP satellite spins at a rate of about 6 rpm. Each satellite of this series is equipped with four deployable solar arrays (Figure 2). From our photometric observations and those conducted by Didenko [16], it has been deduced that the DSP optical system rotates about the optical axis with the period *P1*=10.44 sec. Moreover, the DSP satellite rotates conically around the zenith-nadir axis with the period *P2*= 62.64 sec.

Figure 3 depicts a fragment of the DSP-18 light curve; in 2009, the satellite was relocated from the longitude λ = 145° E to $\lambda \approx 20°$ E whereat we observed it in 2014.

Cosmos 2397. The satellite was launched into geostationary orbit in 2003. Numerous attempts of the GSS to enter normal operating mode failed, and it went into drifting mode two months after launch. We conducted observations of the GSS in September 2004. Two light curves were plotted from observations at small phase angles ψ (that is, the Sun-SO-observer angles) during the GSS passing out of the Earth's shadow through the field of view (FOV) of our observing facility. These two curves are shown in Figure 4 and 5, where Texp is the exposure time for a single measurement.

Figure 2: A DSP satellite model

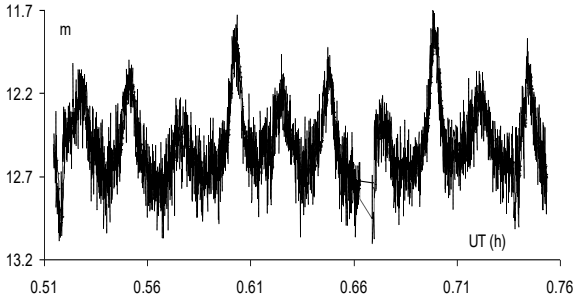

Figure 3: A light curve for DSP-18 observed in the V band on 29 September 2014 with Texp = 0.2 sec

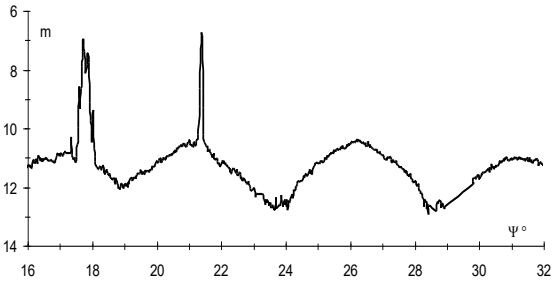

Figure 4: A phase light curve of Cosmos 2397 plotted from observations through a V-filter on 12 September 2004 with Texp = 5 sec.

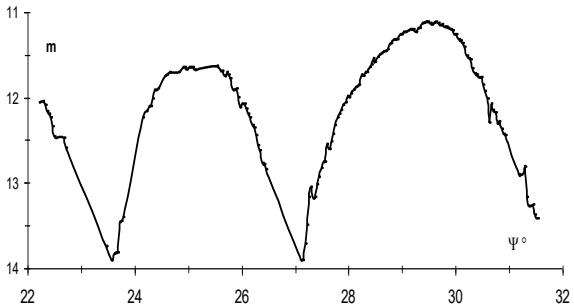

Figure 5: A phase light curve of Cosmos 2397 plotted from observations through a V-filter on 14 September 2004 with Texp = 5 sec.

The most interesting light curve with diffuse and specular reflection components plotted from observations upon the GSS exiting Earth's shadow illustrated in Figure 4. The GSS solar arrays rotate at a maximum rate of one revolution per 18 minutes. When the first and second glints were recorded,

the GSS solar panels were tilted towards the Sun at an angle of 6.5 and 8.7 degrees, respectively.

The minimum tilt angle of the solar panels relative to the Sun was ~5 degrees. This is a typical inclination of solar arrays of an active GSS with respect to the Sun. The solar panel tilt angle with respect to the Sun can be computed from the GSS photometric data. The solar array orientation relative to the Sun remains unaltered despite the GSS keeps drifting slowly along its orbit (~$1^{\mathbf{0}}$ per day). Components of the unit normal to the solar array surface in the satellite-centred reference system, which correspond to the second peak in brightness at the phase angle ψ from $19^{\mathbf{0}}.13$ to $23^{\mathbf{0}}.65$ in the light curve, are given in Table 1. Observing conditions changed slightly during the following night of observations (Figure 5), thus making it only possible to plot a diffuse light curve. As can be deduced from Table 1, the *Y*-component is directed to the centre of the Earth, the *Z*-component is parallel to the Earth's axis of rotation, and the *X*-component is parallel to the celestial equator being directed towards the vernal equinox. Two specular glints plotted in Figure 4 demonstrate that the respective solar panels were perpendicularly to the ecliptic. Thus, the normal orientation was defined as $\alpha = 176^0.96$, $\delta = 4^0.94$ and $\alpha = 179^0.22$, $\delta = 4^0.96$ at the instant of the first and second glint, respectively.

Table 1: The orientation of the normal to the solar-panel surface with respect to the observer at the ψ from $19^0.13$ to $23^0.65$ as recorded on 12 September 2004.

ψ	X	Y	Z
19.130	0.023	0.994	-0.104
20.196	0.013	0.995	-0.096
21.044	0.004	0.996	-0.090
21.413	0.001	0.996	-0.088
21.766	-0.003	0.996	-0.086
22.855	-0.014	0.997	-0.081
23.652	-0.021	0.997	-0.077

In the above Table, ψ is the satellite phase angle; X, Y, Z are components of the normal vector to the reflecting surface in the satellite-centred reference frame. We suggest that entering a non-standard operating mode was most likely caused by the failure to spin-stabilise the GSS, which resulted in its spinning around one of its axes.

SBIRS-GEO 2. The SBIRS-GEO spacecrafts are intended to replace the DSP series. The SBIRS-GEO satellites, built upon the Lockheed Martin A2100M satellite bus, feature two Short Schmidt telescopes and Northrop Grumman infrared payload, including scanning and staring sensors [28]. Each of the SBIRS-GEO spacecrafts employs a scanning sensor that provides a wide-area progressive scanning across large swaths of the Earth's surface (sweep mode) with a short revisit time over its full 14-degree FOV and a starring sensor with a narrow 4-degree FOV, which can be trained constantly for step-stare or dedicated stare operations over smaller areas of interest. The shape of the SBIRS-GEO 2 spacecraft can be seen in Figure 6. The estimated on-orbit dimensions of the GSS make 14.81 x 6.83 x 6.00 m. The longitude of the GSS sub-point is $\lambda = 23°$ E, the orbital inclination $i = 4°.9$ and eccentricity $e = 0.0003$.

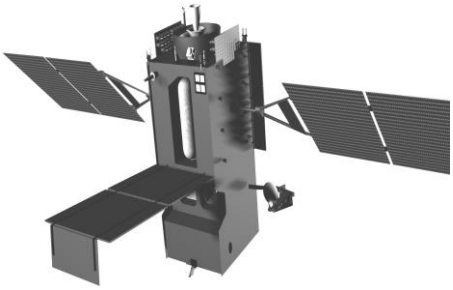

Figure 6: A SBIRS-Geo 2 satellite model.

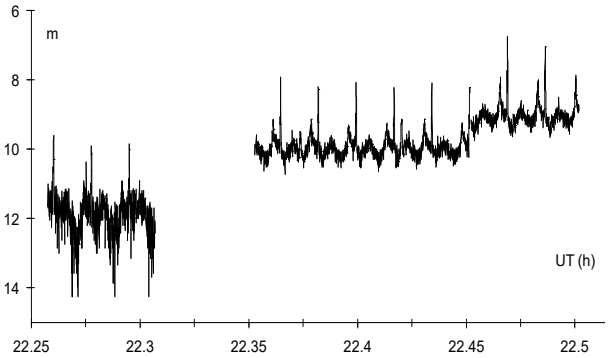

Figure 7: A light curve of SBIRS-Geo 2 observed through BVR filters on 29 August 2014: B (UT = 22.25 – 22.30), V (UT = 22.35 – 22.45), R (UT = 22.45 - 22.50). Texp = 0.1 sec; $\psi = 7°$.

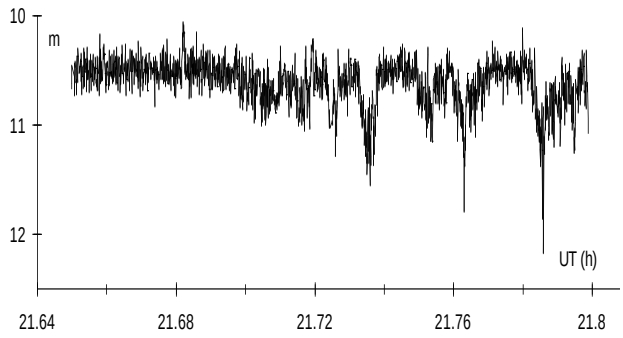

Figure 8: A light curve of SBIRS-Geo 2 observed in the V-band on 01 October 2014. Texp = 0.2 sec; $\psi = 15°$.

A different approach to the Earth's scanning has been implemented in the SBIRS-GEO series as compared with the DSP predecessors. Inside the satellite body, there are two optical telescopes with precisely pointed mirrors, placed in openings on the same side of the platform, which rotate about two axes thus allowing scanning and staring at designated areas. In addition to a pair of two-panel solar arrays, there is an electronics equipment panel attached at the end of the platform at an angle of 90°, which performs a number of specific functions, including calibration of IR receivers.

Over the period from 22 August 2014 to May 2020, the authors obtained about 40 light curves in the BVR bands. Figures 7 and 8 depict the SBIRS-Geo 2 light curves plotted upon our observations at small phase angles ψ.

The most informative light curves in B, V, R band were plotted from observations carried out on 29 August 2014. During that observation night, there was a series of specular glints, with the brightest ones being observed in the R band. However, the most prominent amplitude variations in the brightness were observed through a B filter (Figure 7). With the Sun being west of the SO, no brightness variations were observed in the R band.

Dynamic characteristics of SBIRS-GEO 2. A computational procedure of sequential determination of dynamic characteristics of SBIRS-GEO 2 using its photometric and positional data is described in detail below; the parameters computed at each stage are listed in Table 2.

Table 2: The results of computing dynamic characteristics of SBIRS-GEO 2

No	Parameters	22 August 2014	29 August 2014
1	UT (h m s)	22 34 30 – 22 40 50	22 15 00 – 22 29 40
2	$\alpha^{\odot}$ (°)	151.85	158.25
3	$\delta^{\odot}$ (°)	11.56	9.13
4	α_o (°)	158.95 – 160.54	160.78 – 164.27
5	δ_o(°)	8.37 – 8.23	8.21 – 7.87
6	α_g (°)	159.07 – 160.65	160.93 – 164.43
7	δ_g(°)	1.31 – 1.17	1.16 – 0.85
8	α_n (°)	-	159.51 – 161.27
9	δ_n (°)	-	8.67 – 8.51
10	α_x (°)	249.12 – 250.64	250.48 – 253.98
11	δ_x (°)	2.01 – 2.02	2.06 – 2.08
12	ν (°)	9.41 – 9.80	7.65 – 8.28
13	ψ (°)	7.68 – 9.17	2.67 – 6.08
14	λ (°)	28.95 – 28.94	28.52 – 28.49
15	φ (°)	-1.31 – 1.17	-1.16 – -0.86
16	ω_λ (°/min)	0.0016	0.0017
17	ω_φ (°/min)	0.0233	0.0205
18	λ, φ Odesa	30.27; 46.40	30.27; 46.40

The rows of Table 2 show the next parameters:
Row 1: the SO observing session duration in UT;
Rows 2 and 3: the equatorial coordinates of the Sun;
Rows 4 and 5: the equatorial coordinates of the observer during the observing session;
Rows 6 and 7: the geocentric equatorial coordinates defining the SO orbital position;
Rows 8 and 9: the equatorial coordinates of the normal to the SO glinting surface;
Rows 10 and 11: the equatorial coordinates specifying the SO orbital position;
Row 12: the angle between the SO-Earth's centre line and normal to the SO glinting surface;
Row 13: the phase angle at the specified SO position;
Row 14 and 15: the geodetic longitude and latitude of the SO sub-point during the observing session;
Rows 16 and 17: the velocity of the SO sub-point at the specified geocentric latitude and longitude;
Row 18: the geographic longitude and latitude of the observing site.

The analysis has shown that the shape of the SBIRS-GEO 2 light curves essentially depends on the position of the Sun with respect to the SO (either west or east of the SO), as well as on the SO position relative to the local meridian. The GSS does not only perform diurnal rotation around Earth, but also undergoes libration along the equator within the range of ~ 9°-10°. For instance, the mean longitude was $\lambda \approx 28^0.5$ and $\lambda \approx 20°.6$ during our observing sessions on 29 August 2014 and 3 May 2016, respectively. A significant change in illumination in all three colour-channels occurs when the SO is near the observer's meridian while the Sun illuminates it from eastwards. When the Sun is west of the SO, the SO brightness variations, seen as noticeable dips in Figure 8, occur mainly in the blue and yellow band as the solar arrays are periodically shaded by the IR sensors. The SO brightness variations are observed with a low periodicity when the SO is shifted at some angular distance to the west of the observer's meridian.

At such an orbital position of the SO, its longitudinal axis coincides with the eastward direction of its orbital motion. The side of the platform, wherein openings for mirrors and equipment panel for the IR calibration are located, faces Earth. The light from the SO seen by a ground-based observer is reflected off the solar arrays, equipment panel and satellite body ribs. This is indicative of an oscillatory motion of the GSS and its solar arrays around its longitudinal axis with the period *P2* = 62.64 sec. There is no publicly available information about oscillation motion of the GSS body. When the GSS is near the local meridian when it is crossed by the Sun at its lower culmination, the observer can see specular glints produced by one of the mirrors, deployed at a certain angle to the Northern Hemisphere. Such glints were recorded on 29 August 2014 and could be only observed when the GSS was near the local meridian at $\psi \leq 6°.0 - 6°.5$.

The SO-Sun line and the observer's location specified with the coordinate δ must match within $1^0.5$ for the SO glints to be observable. It is associated with deep-set openings in the platform for the mirrors that rotate rapidly. The period of the mirror rotation is *P1* = 15.66 sec.

Thus, for one complete period of oscillations, that is *P2* = 62.64 sec, the GSS manages to cover the swath four times the width of ~ 9,000 km from the North to the South Pole. Specular glints corresponding to several brightness peaks in the R band observed on 29 August 2014 were not caused by rapidly rotating mirrors. Apparently, they were produced by the equipment panel due to the satellite oscillations upon reaching its maximum northerly deviation. The R-band reflection observed on 29 Aug 2014 was not due to the mirrors' rotation either; these flashes were produced by the equipment panel as a result of the satellite platform oscillations.

The afore-described details enabled us to estimate the angle of oscillation of the satellite body about its longitudinal axis. The angle (ν - δ_g) during the observing session was close to 7°, that is, the GSS underwent oscillations at an angle of $7^0.0–7^0.5$ either side of the axis, thereby extending the monitored area of the Earth's surface covering both polar regions. The DSP satellites, the predecessors to the SBIRS-GEO spacecrafts, are capable to scan the Earth's surface between 83° North and 83° South latitudes. Some photometric characteristics of SBIRS-GEO 2 obtained several observing sessions are listed in Table 3. The effective reflecting area ($S\gamma_\lambda$) was calculated using Equation 2.

Table 3: Photometric characteristics of SBIRS-Geo 2 acquired during several observing sessions.

Date, $\delta^{\odot}$	Sp	m (± 0.05) $\psi = 0°$	m $\psi=25°$	$S\gamma_\lambda$ $\psi=0°$
29.08.2014 $\delta^{\odot}$ =09°07'	И	14.23	14.33	0.128
	M	12.41	12.52	0.377
	K	10.40	10.50	1.49
30.08.2014 $\delta^{\odot}$ = 8°46'	B	13.398	13.505	0.274
	V	9.465	9.573	5.611
	R	10.172	10.28	1.823
01.10..2014 $\delta^{\odot}$= -03°11'	V	12.36	12.47	0.396

The following parameters are presented in the columns in Table 3:
Column 1: date of observations and declination of the Sun;
Column 2: spectral range;
Column 3: the SO reduced magnitude at the phase angle $\psi = 0°$;
Column 4: the SO reduced magnitude at the phase angle $\psi = 25°$;
Column 5: the effective reflecting area ($S\gamma_\lambda$).

When specular glints were observed, each light curve was smoothed as a function of phase for a flat plate with Lambertian scattering. The presence of specular glints in the light curves makes it possible to determine the SBIRS-Geo 2 orientation while in orbit, as well as the SO-Earth's centre line and normal vector, at the instant of the respective glint.

The light-curve fitting procedure was applied to eliminate the effects of specular glints from the computations, and a model of diffuse light scattering from the SO surface was employed at the phase angles close to 0^0.

The procedure for interpreting the diffuse component proposed in [9] was used at zero phase angle, as it was possible to compute the respective value $S\gamma_\lambda$ at $\psi = 0°$. A comparison of colour-indices with those derived from the reflectance spectra of known materials performed by Murtazov *et al.* [9] and Cowardin *et al.* [6], as well as the magnitude *m* observed through different filters (Figure 7), has confirmed that the "red" component dominates in the light reflected from the SO while the "blue' component is brighter when the SO experiences periodic oscillations and its solar arrays are shaded.

A thorough analysis of the light curves and positional data (α, δ) offers considerable scope for studying the behaviour of satellites in geostationary orbits.

4. Conclusions

In Section 3 and Table 2 show the results and unique capabilities of the photometric method for studying SO behavior in orbit. Very few papers have been published in this new and developing field. The following data have been added to our consideration and computation: the Sun's position relative to the SO and observer; the SO position with respect to the local meridian; phase angles; colour-indices; the SO images and plotted light curves; periods of brightness variations; the SO orbital inclination; data reported by other researchers, etc. The algorithm applied in this study is not universally applicable, as it does not yield a common solution in all cases. Moreover, it depends on the amount priori information about the SO. Relevant experience of an expert (researcher) is also of great importance. As stated in reference [26], "light-curve interpretation, however, is more art than science and does not lend itself easily to automation".

The study of in-orbit behaviour has been also performed for some other space objects – namely, EgyptSat 1, Sich 1, Sich 2, Spot 1, Spot 4, Topex/Poseidon as well as other LEO and GEO satellites. The respective findings are reported in [2,18,19] and available in the Ukrainian National Space Facilities Control and Test Centre.

References

1. Yepishev V.P., Isaak I.I., Motrunich I.I., Naybauer I.F., Novak E.I., Tsikavyy A.A.: 2005, *Sbornik trudov "Okolozemnaya astronomiya-2005"*, 267.
2. Yepishev V.P., Motrunich I.I., Naybauyer I.F., Kudak V.I., Perig V.N., Moskalenko S.S., Sukhov P.P., Sukhov K.P.: 2017, *Aerokosmicheskiye tekhnologii*, **№2** (02), 26. http://spacecenter.gov.ua/contents/uploads/2018/08/Part1.pdf
3. Yepishev V.P.: 1983, *Astrometriya i astrofizika. Kiyev, AN USSR*, **№50**, 89.
4. Severnyy S.A., Smirnov M.A., Bagrov A.V.: 1984, *Nauchnyye informatsii*, **58**, 103.
5. Bradley Ben K., Penina Axelrad: 2013, in: *Proc. AMOS Technical Papers*. https://amostech.com/TechnicalPapers ASTRODYNAMICS/BRADLEY.pdf
6. Cowardin H., Seitzer P., Abercromby K., Barker E., Schildknecht T.: 2010, *NASA TechnicalReports Server*. https://ntrs.nasa.gov/search.jsp?R=20110015517
7. Furfaro R., Linares R., Reddy V.: 2018, in: *Proc. AMOS Technical Papers.* https://amostech.com/TechnicalPapers/2018/NROC/Furfaro.pdf
8. Krantz Harisson, Pearce Eric C., Avner Louis, Rockowitz Kris: 2018, in: *Proc. AMOS Technical Papers*. https://amostech.com/TechnicalPapers/2018/Optical-Systems_Instrumentation/Krantz.pdf
9. Murtazov A.: 2013, *American Journal of Modern Physics*, **2(6)**, 282. DOI: 10.11648/j.ajmp.20130206.12
10. Payne Tamara E, Castro Philip J., Gregory Stephen A., Phan Dao: 2015, in: *Proc. AMOS TechnicalPapers*, Kihei, Maui, HI. Technical Papers. https://amostech.com/TechnicalPapers/2016/NROC/Payne.pdf
11. Schmitt Henrique R., Vrba Frederick J.: 2016, in: *Proc. AMOS Technical Papers*. https://amostech.com/TechnicalPapers/2016/Poster/Schmitt_01.pdf
12. Sukhov P.P., Kouprianov V.V., Sukhov K.P.: 2017, in: *Proc. 7th European Conference on Space Debris, Darmstadt, Germany, Confer.proceed.* 18. https://conference.sdo.esoc.esa.int/proceedings/sdc7/paper/363/SDC7-paper363.pdf
13. Sukhov P.P., Karpenko G.F., Sukhov K.P., Epishev V.P., Motrunych I.I., Kudzej I., Dubovsky P.A.: 2014, *Odessa Astron. Publ.*, **27/2**, 149. https://pdfs.semanticscholar.org/8ec2/13d3bd76b87eb626f047f8c784e02e5cf31a.pdf
14. Vrba Frederick J., DiVittorio Michael E., Hindsley Robert B., Schmitt Henrique R., Armstrong J. Thomas, Shankland Paul D., Hutter Donald J., Benson James A.: 2009, in: *Proc. AMOS Technical Papers*.

https://amostech.com/TechnicalPapers/2009/Non-resolved_Object_Characterizaion/Vrba.pdf
15. Vygon Vadim, Shargorodskiy V.D.: 2009, *AMOS Abstracts of technical papers*, 21, http://www.bitnet.info/proiecte/leoscop/2009amosabstracts.pdf
16. Didenko A.V., Usol'tseva L.A.: 2010, *Izvestiya NAN RK*, **№4**, 81, http://lfvn.astronomer.ru/report/0000068/dsp_23_didenko_usoltseva.pdf
17. Didenko A.V., Usol'tseva L.A.: 2006, *Izvestiya NAN RK. Seriya fiz.-mat.*, **№4**, 100, http://www.astronomer.ru/publications.php?act=view&id=170
18. Yepíshev V.P., Sukhov P.P., Motrunich Í.Í., Kashuba V.Í., Kudak V.Í., Períg V.M., Sukhov K.P., Naybauer Í.F.: 2018, *Naukoviy vísnik Uzhgorodskogo uníversitetu. Seríya Fízika*, **43**, 54. DOI: https://doi.org/10.24144/2415-8038.2018.43.54-62.
19. Sukhov P.P., Yepishev V.P., Sukhov K.P., Karpenko G.F., Motrunich I.I.: 2017, *Kosmíchna nauka i tekhnologíya*, **23**. №1, 63. DOI: https://doi.org/10.15407/knit2017.01.063
20. Shabarekh Charlotte, Keselman Gene, Kent-Bryant Jordan, Mitidis Andonis, Baldwin Jason, Engberg Brian: 2016, *AMOS Abstract and TechnicalPapers.* https://amostech.com/TechnicalPapers/2016/SSA/Shabarekh.pdf
21. Christopher R. Binz, Mark A. Davis, Bernie E. Kelm, Christopher I. Moore: 2014, in: *Proc. AMOS TechnicalPapers*, https://amostech.com/TechnicalPapers/2014/Poster/BINZ.pdf
22. Toyaj Singh: 2019, https://arxiv.org/pdf/1910.10847.pdf
23. Andy Speicher: 2015, https://digitalcommons.du.edu/etd/1050/
24. Tikhonov A.N., Arsenin V.Ya.: 1979, Metody resheniya nekorrektnykh zadach. Izd. 2. Moskva: Nauka, 142p. http://bookre.org/reader?file=442750&pg=3
25. Sukhov P.P., Chaychuk R.A.: 1984, *Novaya tekhnika v astronomii. AN SSSR*, 20.
26. Kornilov V.G., Volkov I.M., Zakharov A.I., Kozyreva B.S., Kornilova L.N., Krutyakov A.N., Krylov A.V., Kusakin A.V., Leont'yev S.Ye., Mironov A.V., Moshkalev V.G., Pogrosheva T.M., Sementsov V.N., Khaliullin G.F.: 1991, *Katalog WBVR-velichin yarkikh zvezd severnogo neba* /ed. V.G.Kornilova. Trudi GAISH. T.63. M.: Izd-vo Moskovskogo un-ta. 400 p.
27. https://en.wikipedia.org/wiki/Fobos-Grunt
28. https://mapgroup.com.ua/kosmicheskie-apparaty/26-kosmicheskie-apparaty-ssha/1808-sbirs-geo-1-2-3-4